Solution-Processed Ferroelectric Terpolymer Nanocomposites with Large Breakdown Strength and High Energy Density Utilizing Boron Nitride Nanosheets

Journal:	*Energy & Environmental Science*
Manuscript ID:	EE-ART-09-2014-002962.R2
Article Type:	Paper
Date Submitted by the Author:	18-Nov-2014

Complete List of Authors:	Li, Qi; The Pennsylvania State University, Materials Science and Engineering Zhang, Guangzu; The Pennsylvania State University, Materials Science and Engineering Liu, Feihua; Wuhan University of Technology, Materials Science and Engineering Han, Kuo; The Pennsylvania State University, Materials Science and Engineering Gadinski, Matthew; The Pennsylvania State University, Materials Science and Engineering Xiong, Chuanxi; Wuhan University of Technology, Materials Science and Engineering Wang, Qing; The Pennsylvania State University, Materials Science and Engineering

Cite this: DOI: 10.1039/c0xx00000x

www.rsc.org/xxxxxx

ARTICLE TYPE

Solution-Processed Ferroelectric Terpolymer Nanocomposites with High Breakdown Strength and Energy Density Utilizing Boron Nitride Nanosheets

Qi Li,[a,#] Guangzu Zhang,[a,b,#] Feihua Liu,[c] Kuo Han,[a] Matthew R. Gadinski,[a] Chuanxi Xiong[c,*] and Qing Wang[a,*]

Received (in XXX, XXX) Xth XXXXXXXXX 200X, Accepted Xth XXXXXXXXX 200X
DOI: 10.1039/b000000x

The development of high-performance capacitive energy storage devices is of critical importance to address ever-increasing electricity need. The energy density of a film capacitor is determined by the dielectric constant and breakdown strength of dielectric materials. With the highest dielectric constant among the known polymers, poly(vinylidene fluoride)-based ferroelectric terpolymers are of great potential for high energy density capacitors. However, their energy storage capability has long been limited by the relatively low breakdown strength. Here we demonstrate remarkable improvements in the energy density and charge-discharge efficiency of the ferroelectric terpolymers upon the incorporation of ultra-thin boron nitride nanosheets (BNNSs). It is found that BNNSs function as a robust scaffold to hamper the onset of electromechanical failure and simultaneously, as efficient insulating barrier against electrical conduction in the resulting polymer nanocomposites, resulting in greatly enhanced breakdown strength. Of particular note is the improved thermal conductivity of the terpolymer with the introduction of BNNSs; this is anticipated to benefit the stability and lifetime of polymer capacitors. This work establishes a facile, yet efficient approach to solution-processable dielectric materials with performance comparable or even superior to those achieved in the traditionally melt-extruded ultra-thin films.

Broader context

With increased energy production from solar and wind, energy storage technologies are crucial for efficient utilization of the electricity generated from these intermittent, renewable sources. Among currently available technologies for electrical energy storage, film capacitors possess intrinsic advantage of high power densities and fast charge/discharge rate, yet they are considerably limited by energy densities that are much lower than those of the electrochemical energy storage devices such as batteries. This work presents a nanocomposite approach based on boron nitride nanosheets to the state-of-the-art ferroelectric polymers, which leads to greatly improvement in energy densities and energy discharge capability. The excellent performance along with the simplicity and scalability of preparation makes the ferroelectric polymer nanocomposites promising candidates for compact and flexible high-energy high-power capacitive energy storage devices.

1. Introduction

The exploitation of high-performance, easily-processed, lightweight and cost-effective materials has been at the central place of the development of electrical energy storage and conversion technologies required by the implementation, miniaturization and integration of advanced electronic devices.[1] Dielectric materials can store and release electrical energy through dielectric polarization and depolarization by the application and removal of electric fields, and thereby enable the dielectric capacitor technology. Capacitors are basic components in electronic and electrical systems such as portable electronics, medical defibrillators, hybrid electric vehicles and power grids. Dielectric capacitors store energy electrostatically in an electric field and possess the intrinsic fast charge-discharge capability to offer the highest power density and longest lifetime among all currently available electrical energy storage devices,[2,3] which is crucial for power electronics, power conditioning, and power conversion. However, they are limited by the amount of energy that can be stored in dielectric materials. For example, the energy density of the best commercially available film capacitors represented by biaxially oriented polypropylenes (BOPP) is usually at least one order of magnitude lower than those of the electrochemical supercapacitors and batteries on the market.[4-6]

Significant improvements in energy density would enable the reduction in size, weight and cost of the power systems.

The stored energy density (U) of a dielectric capacitor is determined by the applied electric field (E) and the induced electric displacement (D) within the dielectric materials sandwiched between two electrodes, as expressed by $U = \int EdD$ (see Supplementary Fig. S1 for schemetic representation). In particular, U scales quadratically with E and linearly with dielectric constant in linear dielectrics following the eqation $U = ½DE = ½K\varepsilon_0E^2$, where K is the dielectric constant and ε_0 is the vacuum permittivity. Apparently, as the breakdown strength (E_b) signifies the maximum E that can be applied on a dieletric material, E_b becomes the most critical parameter that defines the U value of capacitors. One example is that, although the K value (~2.2) of BOPP, is hundreds to thousands times lower than those (usually at the level of 10^3-10^4) of typical ceramic capacitors, such as barium titanate,[7] they share a very similar U of ~5 J cm^{-3}, owing to the superior E_b of BOPP (700 MV m^{-1}) when compared to those of the ceramic films, *i.e.*, ~80 MV m^{-1}.

Poly(vinylidene fluoride) (PVDF)-based ferroelectric polymers are considered as the most promising class of dielectric materials for high energy denisty capacitors because of their unique combination of high E_b and large K.[8-10] The strong polarization arising from C-F bonds and the spontaneous alignment of dipoles in the crystalline phases give rise to PVDF based polymers with higher K relative to non-ferroelectric polymers whose room-temperatue K is far less than 10. The solution-cast thin films of ferroelectric copolymers such as poly(vinylidene fluoride-*co*-chlorotrifluoroethylene), P(VDF-CTFE), with K values around 10 at 1 kHz, display energy densities of 7-8 J cm^{-3} at an E_b of ~400 MV m^{-1}.[11,12] Substantially higher energy densities of 17-25 J cm^{-3} has been obtained in the ferroelectric copolymer thin films such as P(VDF-CTFE) and P(VDF-HFP) (poly(vinylidene fluoride-*co*-hexafluoropropylene) manufactured from melt-stretching and extrusion-blowing processes.[10,13,14] The melt stretching-based methods improve mechanical properties and reduce ionic conduction of thin films, leading to radically increased E_b values, *e.g.* >570 MV m^{-1}, with respect to the solution-cast films, which directly translates to greater energy densities. On the other hand, it is worthwhile to point out that the stretching inevitably promotes a partial conversion of non-polar α-phase in PVDF to polar β-phase. This results in high remnant polarization and large ferroelectric loss, and accordingly, decreases the charge-discharge efficiency of capacitors (defined as U_e/U, where U_e denotes discharged energy density, see Supplementary Fig. S1).[15]

A unique class of PVDF-based ferroelectric polymers is the terpolymers including poly(vinylidene fluoride-*ter*-trifluoroethylene-*ter*-chlorotrifluoroethylene), P(VDF-TrFE-CTFE), and poly(vinylidene fluoride-*ter*-trifluoroethylene-*ter*-chlorofluoroethylene), P(VDF-TrFE-CFE), which enjoy the highest room-temperature K values (*i.e.* ~50 at 1 kHz) among the known dielectric polymeris.[16,17] The incoporation of the third monomers such as CTFE and CFE containing slightly bulky chlorine atoms into P(VDF-TrFE)s moves the Curie transition to near ambient temperature by reducing the crystalline domain size and the energy barrier in phase transition, and converts the normal ferroelectrics of the copolymes to a ferroelectric relaxor.[18] The terpolymer with high reversible polarization indicated by a narrow polarization loop and a large electrical displacement exhibits an electrical energy density of ~9 J cm^{-3} at 400 MV m^{-1}.[19] However, the presence of CTFE and CFE as defects unfortunately degrades the mechanical strength of the polymers. For example, the Young's modulus of P(VDF-TrFE-CFE) is only around 150 MPa, compared to ca. 800 MPa of P(VDF-HFP).[14] As dielectric breakdown of ferroelectric polymers are mainly governed by the electromechnical mechanism,[20] the inferior mechanical properties of the terpolymers result in much lower E_b (*i.e.* < 400 MV m^{-1}) in comparison to those of the ferroelectric copolymers. Moreover, these terpolymers are found to be too soft to be effectively processed into ultra-thin film (*i.e.* <10 μm) with enhanced dielectric strength by using the most common melt-extrusion or streteching methods. Therefore, even though these terpolymers have the highest K values, their potential for high energy density capacitors has not been fully exploited due to limitations in E_b as aforementioned.

Herein we describe a nanocomposite approach based on ultra-thin boron nitride nanosheets (BNNSs) toward ferroelectric P(VDF-TrFE-CFE) terpolymer exhibiting significantly improved E_b in comparison to the pristine terpolymer. This is distinctively different from most of the coventional dielectric nanocomposites,[21,22] in which the introduction of inorganic nanofillers normally lowers E_b. The improvement in E_b of PVDF-based polymers has been previously achieved by aligning inorganic nanofilers, such as SiO_2 nanoparticles,[23,24] montmorillonite nanoplates,[25,26] and kaolinite clay nanofillers,[27] in the polymer matrix via mechanical stretching. However, the increased E_b is typically accompanied by the decrease in the charge-discharge efficiency. In this work, marked improvements in energy storage and discharge capability associated with elevated E_b have been demonstrated in P(VDF-TrFE-CFE)/BNNS nanocomposites. Notably, compared to the state-of-the-art dielectric thin films processed by melt-extrusion and stretching methods, the solution-processed polymer nanocomposites not only display a similar level of energy density and E_b but also present reduced dielectric loss and much higher charge-discharge efficiencies under the applied fields.

2. Experimental

2.1. Methods

Preparation of BNNSs: BNNSs are chemically exfoliated in DMF following a sonication-centrifugation process.[28-30] Typically, 2g *h*-BN powders (Sigma-Aldrich) were dispersed in 150 mL DMF (Sigma-Aldrich) under vigorous stirring. The mixture was then subjected to a 48-h tip-type sonication (175 W, 500 W×35%). The resultant mixture was first centrifuged at 3,000 rpm for 40 min, and the supernatant was collected. This step purified the mixture from un-exfoliated *h*-BN powders. Then the supernatant was subjected to a 20-min centrifugation at 10,000 rpm to precipitate BNNSs. After vacuum drying overnight at 70 ^{o}C, BNNSs were obtained.

Synthesis of P(VDF-TrFE-CFE)s: The systhesis of terpolymer follows a literature work.[18,31,32] Deionized water and potassium peroxodisulfate (VWR) initiator was added to a stainless steel vessel which was subsequently sealed and degassed via vacuum pump and cooled using liquid nitrogen bath. Gaseous VDF, TrFE

and CFE (SynQuest Laboratory Inc.) were pumped into the reaction vessel separately with the amount varied by time to control composition. The vessel was heated at 90 ^{o}C for 12 h. After this time, the volatiles were vented, and subsequent precipitation into methanol, washing by hexane, and drying in vacuo, afforded a white solid identified as P(VDF-TrFE-CFE). 1H NMR (DMSO-d_6, ppm): δ 2.2-2.5 (m, 2H, -CH_2-CH_2-, VDF and CFE tail to tail segments), 2.6-3.6 (m, 2H, -CH_2-, VDF and CFE head to head segments), 5.4-6.1 (m, H, -CF*H*-, TrFE segments). ^{19}F NMR (DMSO-d_6, ppm) δ -92.5 (s, 2F, -CF_2-CH_2-CF_2-CH_2-CF_2-, VDF-VDF tail to head linkages), -93.3 6 (s, 2F, -CHF-CH_2-CF_2-CH_2-CF_2- TrFE-VDF tail to tail linkages), -93.5 (s, 2F, -CClF-CH_2-CF_2-CH_2-CF_2-, CFE-VDF tail to tail linkages), -100 to -112 (m, 2F, -CF_2-CFCl-, VDF/TrFE-CFE head to tail linkages), -114.2 (m, 2F, -CF_2-CH_2-CF_2-CF_2-CH_2-, VDF-VDF head to head), -116.5 (m, 2F, -CH_2-CF_2-CF_2-CH_2-CH_2-), -121.7 (s, 2F, -CF_2-CHF-CF_2-CHF-CH_2-, TrFE-TrFE head to tail linkage), -122.8 (d, 2F, -CF_2-CHF-CF_2-CHF-CH_2-), -129.9 (m, 2F, -CH_2-CF_2-CF_2-CHF-CH_2-), -130.9 (m, 2F, -CF_2-CFCl-CF_2-CHF-CH_2-), -195.5 (s, F, -C*F*Cl-), -199 (m, F, -CF_2-CF_2-CH*F*-CH_2-CF_2-), -212 (m, F, -CH_2-CF_2-CH*F*-CF_2-CH_2-). The composition of the P(VDF-TrFE-CFE) is 59.2/33.6/7.2 mol.%.

Fabrication of P(VDF-TrFE-CFE)/BNNS nanocomposites: Typically, P(VDF-TrFE-CFE) powders were dissolved in DMF before filterring through a glass fiber filter (0.7 μm pore size), and stirred overnight to give a homogeneous solution at concentration of 50 mg mL^{-1}. The BNNS dispersion was prepared at concentration of 4 mg mL^{-1} in DMF by tip-type sonication (175 W, 500 W×35%) for 1 h, which was then mixed in the required ratio with P(VDF-TrFE-CFE) solution. After vigorously stirring overnight, the suspension was then subjected to a 30-min tip-type sonication (175 W, 500 W×35%) before drop casting on glass plates. The cast films were first dried at 90 ^{o}C for 6 h, and subsequently peeled off the glass plates for further drying in vacuum at 110 ^{o}C overnight to remove trace solvent. The loading of BNNSs in the nanocomposites was further confirmed by thermogravimetric analysis (TGA, Supplementary Fig. S2). The typical thickness of the nanocomposite films is around 15 μm, and can be tuned by varying the concentraion of the suspensions.

2.2. Characterization

TEM (Joel JEM-2001F) images were obtained by placing a few drops of the dispersion on a lacey carbon covered copper grid, and evaporating them at room temperature prior to observation. SEM measurements were performed with a Hitachi S-4800 field emission electron microscope. Gold electrodes of a diameter of 3 mm and a thickness of 60 nm were sputtered on both sides of the polymer films for the electrical measurements. Dielectric constant and loss were measured using an Agilent LCR meter (E4980A). Resistivity were obtained under an electric field provided by a Hewlett Packard 4140B pA meter/voltage source and KEPCO BOP 1000M amplifier. High-field *D-E* loops were collected using a modified Sawyer-Tower circuit, where the samples were subjected to a triangular unipolar wave with a frequency of 10 Hz. Dielectric breakdown strength measurements were performed on a TREK P0621P instrument using the electrostatic pull-down method under a DC voltage ramp of 500 V s^{-1}. Tensile mechanical testing was carried out on an Instron 5866 using a 200 N load cell and an extension rate of 20 mm min^{-1}. FTIR spectra were obtained in the attenuated total reflectance (ATR) mode using ZnSe crystal as a contact to the samples on Varian Digilab FTS-8010 spectrometer. DSC was conducted by using a TA Instrument Q100 differential scanning calorimeter at a heating and cooling rate of 10 ^{o}C min^{-1}. X-ray diffraction analysis was studied by use of PANalytical X'pert Pro MPD theta-theta diffractometer. All data were analyzed using Jade software with a Gaussian-Lorentz superposition fitting function. TGA measurements were performed with a simultaneous thermal analyzer (Netzsch, STA 499C) at a heating rate of 10 °C min^{-1} under N_2 flow. See Supplementary Information for the method of thermal conductivity measurement.

3. Results

3.1. Preparation of BNNSs and the nanocomposites

BNNSs are prepared through liquid exfoliation method[28-30] from bulk hexagonal boron nitride (*h*-BN) and selected as the fillers to form P(VDF-TrFE-CFE)/BNNSs nanocomposites. *h*-BN, the most stable crystalline form of boron nitride (BN), is a layered van der Waals crystal similar to graphite. Such 2D crystal with strong B-N covalent sp^2 bonds in the plane is able to display the advantages of the (002) face of a graphitic-like structure such as high mechanical strength and thermal conductivity,[28] i.e., *h*-BN is reported to be only second to single-layer graphene in terms of in-plane stiffness[33] and has a thermal conductivity equally good to graphite.[34] *h*-BN is a wide band gap insulator with dielectric permittivity ranging from 3-4 and breakdown strength around 800 MV m^{-1} (refs. 35 and 36). More interestingly, the breakdown voltage of h-BN can be further promoted by decreasing the thickness of h-BN sheet down to few layers, motivating the applications of BNNSs as a dielectric layer in nanoelectronics.[37]

Liquid exfoliation via a sonication-centrifugation process affords ultra-thin BNNSs that can form stable suspensions in DMF without any chemical modification, even at a relatively high concentration (i.e. 4 mg mL^{-1}, Fig. 1a, inset), which is attributable to the polar surface of BNNSs induced by B-N bonds.[28] This also allows TEM observation of individual free-standing BNNS directly deposited from DMF suspension. A dark field TEM image shown in Figure 1a gives the typical morphology profile of an individual BNNS with lateral size of approximately 400 nm. To determine the thickness of the BNNS, an exposed edge is zoomed-in under high-resolution TEM as exhibited in Figure 1b. It is clear that the BNNSs consisting of 4 layers are 2-nm thick, and the electron diffraction pattern (Fig. 1b, inset) validates the hexagonal symmetry nature of BNNSs. Statistical analysis (Figs. 1c and 1d) over a sample set of 34 pieces of BNNSs indicates that majority of the nanosheets are about 2 nm (4-layer sheets) in thickness and 400 nm in lateral size. The productivity of the few-layered BNNSs in this work is approximately 2.5%, i.e. every 2 g of BN powders yield ~50 mg of BNNSs. It is reported that on scale-up to a 10 m^3 of liquid volume in a shear exfoliation method, production rates can exceed 100 g h^{-1} for the preparation of 2-D nanostructures.[38] This would help to realize large-scale production of the composites.

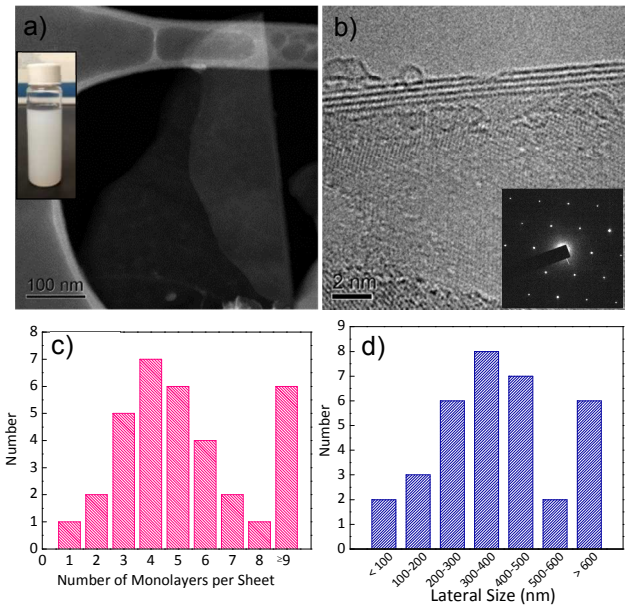

Fig.1 (**a**) Dark field TEM image of BNNS. Inset, BNNSs dissolved in DMF at a concentration of 4 g mL^{-1}. (**b**) High-resolution TEM image of BNNS with 2-nm-thickness. Inset, electron diffraction pattern displaying a hexagonal symmetry. (**c**) Statistic analysis on the number of monolayers per sheet of a set of BNNSs. (**d**) Statistic analysis on the lateral size of a set of BNNSs.

With a polar surface, a proper fraction of bare BNNSs are also found to be readily dispersed in a matrix of polar polymer to afford uniform nanocomposite films via a simple solution casting technique. This is confirmed in our studies by a large-scale cross-section SEM image of P(VDF-TrFE-CFE)/BNNSs nanocomposites, as a homogeneous distribution of BNNSs within the terpolymer is evident up to 12 wt.% loading (Figure 2a). Since BNNSs are of high aspect ratio and specific surface area, they would form a dense network-like microstructure in the polymer matrix upon a drop-casting process (Fig. 2c), which is verified in the simulation studies as presented in Supplementary Fig. S3. By increasing the filler concentration beyond 12 wt.%, aggregation of BNNSs is seen in the nanocomposite as a result of the densely stacking of the nanosheets (Supplementary Fig. S4). The top-view (Fig. 2b) and cross-section (Fig. 2c) SEM images at higher magnification of the nanocomposite sample with 12 wt.% filler also suggest that BNNSs merge well into the host matrix, demonstrating a good compatibility of the inorganic and organic phases. Note that this is attained with unmodified BNNSs, which stands in sharp contrast to conventional polymer nanocomposites that usually require surface functionalization of inorganic fillers to achieve uniform filler dispersion in polymer matrix. This not only would simplify the fabrication of the polymer nanocomposites by eliminating the step of chemical modification but also is beneficial to the breakdown strength of the polymer nanocomposites. In the cases of dielectric nanocomposites, the ligands used in surface modification are typically long hydrocarbon chains, which become the most vulnerable local region to voltage due to their lowest K in comparison to the high-*K* ferroelectric polymer and inorganic dopant phases.[39] The large difference in *K* leads to highly inhomogeneous distribution of local electric fields in nanocomposites, and accordingly, degrades overall dielectric strength.[38]

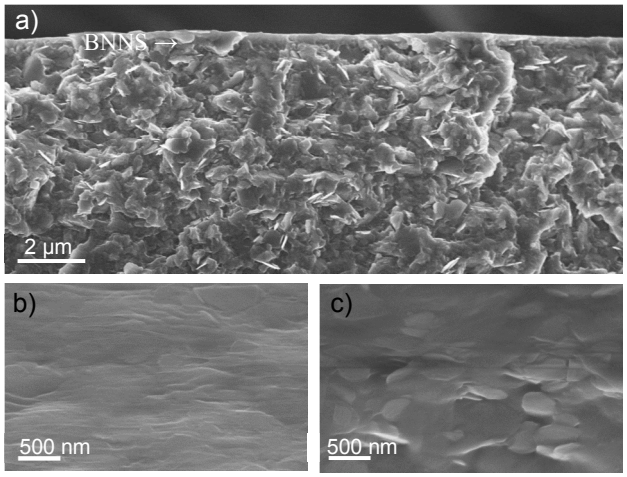

Fig.2 (**a**) Large-scale cross-section SEM image of P(VDF-TrFE-CFE)/BNNS composite film with 12 wt.% BNNSs. (**b**) Zoom-in top-view and (**c**) cross-section SEM images of P(VDF-TrFE-CFE)/BNNS composite film with 12 wt.% BNNSs.

3.2. Breakdown strength of the nanocomposites

Dielectric breakdown strength of the pristine terpolymer and the nanocomposites is analyzed by a two-parameter Weibull statistic described as $P(E) = 1 - \exp(-(E_b/\alpha)^{\beta})$, where $P(E)$ is the cumulative probability of electric failure, E_b is the measured breakdown field, scale parameter α is the field strength for which there is a 63% probability for the sample to breakdown (Weibull E_b), and shape parameter β evaluates the scatter of data. A higher value of β stands for less scattering in the experimetal data. At least 15 tests per sample are carried out to extract the Weibull E_b. The results are plotted as probability density $f(E)$ versus electric field (Fig. 3a): $f(E) = \beta\alpha^{-\beta}E_b^{\beta-1}\exp[(-E_b/\alpha)^{\beta}]$. As shown in Figure 3b, the Weibull E_b of the terpolymer nanocomposites reaches the highest value of 610 MV m^{-1} at the BNNS filler content of 12 wt.%, which represents a 70% increment as compared with that of the pristine terpolymer, *i.e.* 362 MV m^{-1}. Meanwhile, a marked increase of β value from 8.44 in pristine P(VDF-TrFE-CFE) to 15.8 in the nanocomposite filled with 12 wt.% of BNNSs is found (Fig. 3b), suggesting vastly improved dielectric reliability of the nanocomposites. It is also found that film thickness plays a minor role in determing the breakdown strength within the range from 4-25 μm (Supplementary Fig. S5). For the purpose of comparison, in addition to the solution-cast P(VDF-TrFE-CFE) films, the melt-stretched P(VDF-TrFE-CFE) films (Supplementary Fig. S6) are prepared by using zone-heated uniaxially stretching since this process has yielded so far the best ferroelectric copolymer capacitor films in the laboratories.[13,14] A E_b of 507 MV m^{-1} is observed in the melt-stretched P(VDF-TrFE-CFE) films. Notably, the achieved E_b of solution-cast P(VDF-TrFE-CFE)/BNNSs nanocomposites is comparable to those of melt-stretched P(VDF-CTFE) and P(VDF-HFP) thin films,[10,13,14] signifying that a similar level of performance as achieved in the traditionally melt-stretching processed dielectric films are now accomplished in solution-processable dielectric materials.

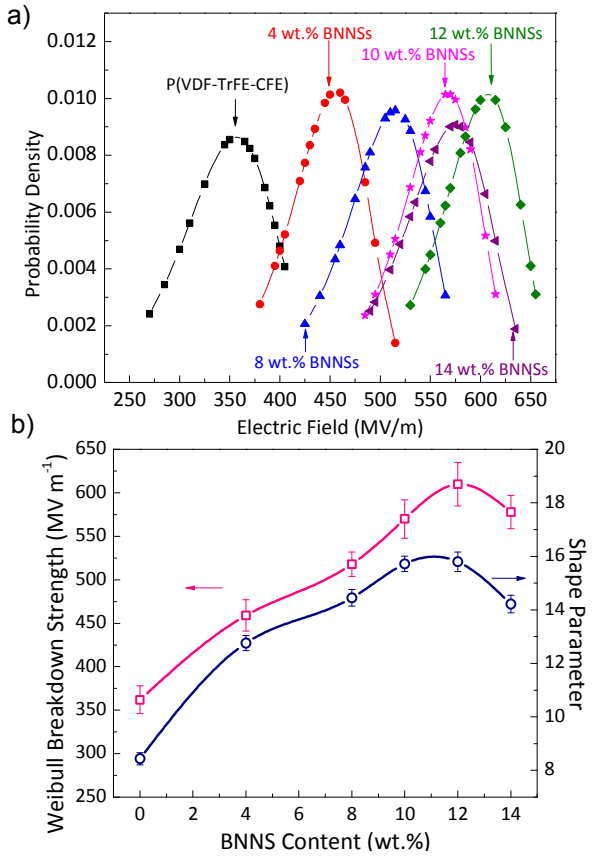

Fig.3 (**a**) Weibull plots for P(VDF-TrFE-CFE)/BNNS nanocomposites with various BNNS contents. (**b**) Weibull breakdown strength (scale parameter) and shape parameter as functions of BNNS fraction.

3.3. Characterizations of electrical energy storage capability

The electric displacement-electric field (*D-E*) loops of a series of P(VDF-TrFE-CFE)/BNNS nanocomposites and the pristine terpolymer are obtained by a modified Sawyer-Tower circuit (Figs. 4a, b and c). The discharged energy density (U_e) is derived from the *D-E* loop by integration of the area between the discharge curve and the ordinate as indicated in the schematic *D-E* loop (Supplementary Fig. S1). As plotted in Figure 4d, U_e can reach up to 20.3 J cm^{-3} from the 15-μm thick terpolymer nanocomposite films with 12 wt.% of BNNSs at 650 MV m^{-1}, which represents a 121% improvement over the solution-cast terpolymer measured at 400 MV m^{-1}. The U_e of the polymer nanocomposite is also greater than that of the melt-stretched P(VDF-TrFE-CFE) which possesses a maximum U_e of ~13.8 J cm^{-3} at 575 MV m^{-1} (with the Weibull E_b at 507 MV m^{-1}). As a matter of fact, the U_e achieved in the present nanocomposite, to our knowledge, is one of the highest recorded for solution-processed dielectric capacitor films in the literature, which also rivals the state-of-the-art reported from the extrusion-blown ferroelectric copolymer ultra-thin films with thickness less than 10 μm, *e.g.* a U_e of 22.3 J cm^{-3} measured at 650 MV m^{-1} from ~5-μm thick P(VDF-HFP) thin films.[14] Importantly, it should be noted that the charge-discharge efficiency of the stretched ferroelectric copolymers has been found to be relatively low,[40,41] as a result of the partially converted crystal structures from non-polar to polar phases that leads to large hysteresis and associated ferroelectric loss. For instance, the charge-discharge efficiency of the extrusion-blown and melt-stretched P(VDF-HFP) is around 65% at 600 MV m^{-1}, and even lower at low electric fields, *e.g.* at 300 MV m^{-1}, the efficiency of P(VDF-HFP)s is only ~57% because of field-dependent loss mechanisms.[41] On the other hand, P(VDF-TrFE-CFE)/BNNS nanocomposite shows significantly higher charge-discharge efficiencies, *i.e.*, ~83% at 300 MV m^{-1} and ~80% at 600 MV m^{-1} (Fig. 4d), which is resulted from the reduced dielectric loss under the applied fields. Besides U_e, the charge-discharge efficiency is another important metric of dielectric materials for energy storage capacitors, as the unreleased energy generates heating and consequently, is detrimental to the performance and reliability of capacitors.

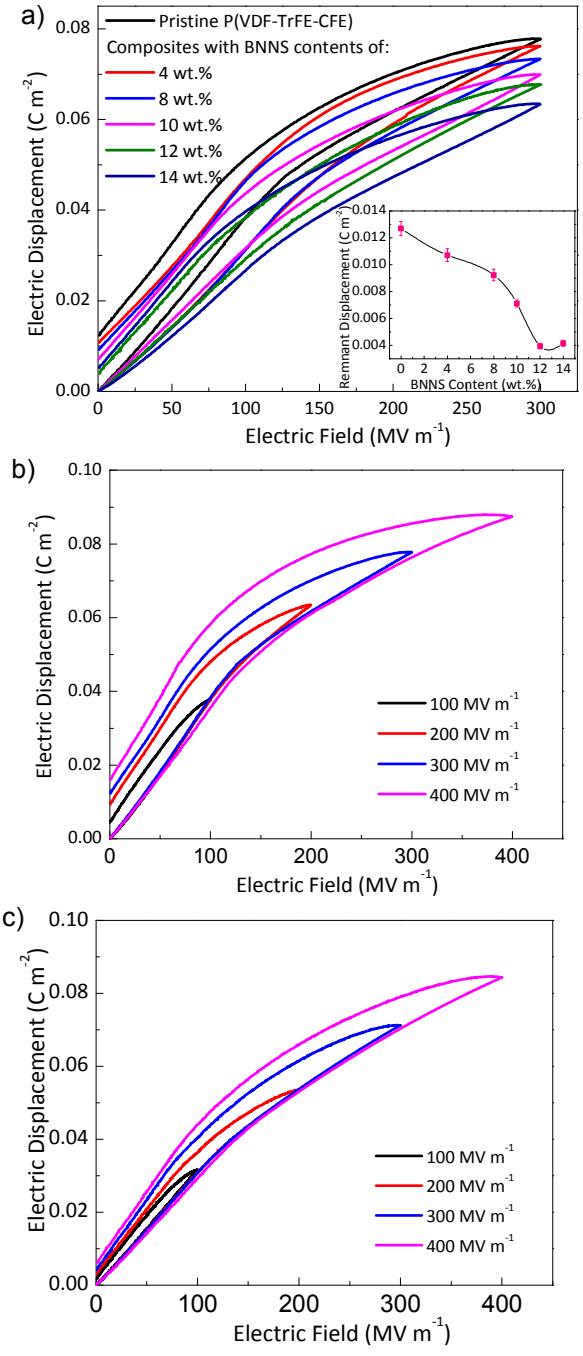

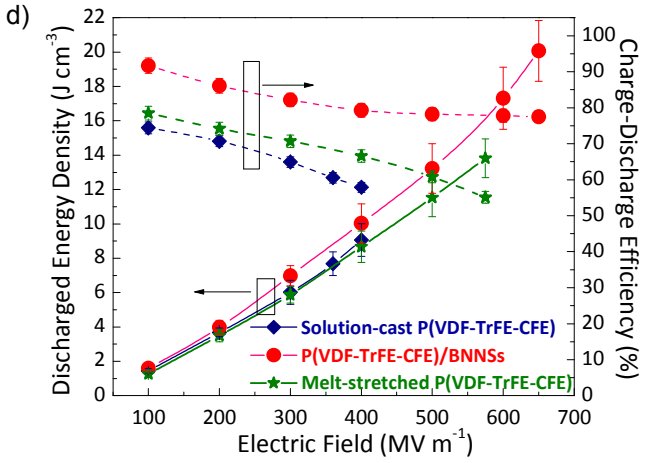

Fig.4 (**a**) Comparison of *D*-*E* loops of pristine P(VDF-TrFE-CFE) and a series of P(VDF-TrFE-CFE)/BNNS nanocomposites at an electric field of 300 MV m^{-1}. Inset: Remnant displacement of P(VDF-TrFE-CFE)/BNNS nanocomposites as a function of filler content. *D*-*E* loops of (**b**) pristine P(VDF-TrFE-CFE) and (**c**) P(VDF-TrFE-CFE)/BNNS nanocomposite with 12 wt.% of BNNSs at varied electric fields. (**d**) Comparison of discharged energy density and charge-discharge efficiency of pristine P(VDF-TrFE-CFE) and P(VDF-TrFE-CFE)/BNNS nanocomposite with 12 wt.% of BNNSs at different electric fields.

The dielectric loss in ferroelectric materials including those from electrical conduction and polarization hysteresis caused by irreversible dipoles is manifested directly by the remnant displacement (*i.e.* the electric displacement at zero electric field). It is apparent that the remnant displacement decreases drastically from 0.013 C m^{-2} of the pristine terpolymer to only 0.004 C m^{-2} of the terpolymer nanocomposite with 12 wt.% of BNNSs (Fig. 4a), and much slimmer loops of the nanocomposite in comparison to those of the pristine terpolymer are clearly seen at respective electric fields (Figs. 4b and 4c). A further increase of BNNS content leads to a slightly increased remnant displacement, presumably due to aggregation of BNNSs. The maximum electric displacement also decreases systematically with increasing feeding ratio of BNNSs, due to the relatively lower K of BNNSs than the terpolymer, which is consistent with the results from weak field permittivity measurement (Supplementary Fig. S7). It should be emphasized that a properly reduced K value does not scarify the ultimate energy storage capability of the nanocomposites, but rather, avoids early *D*-saturation (*i.e.*, polarization saturation occurs at a field far below the breakdown field), which enables films to store more electrical energy at high fields. For instance, as illustrated in Supplementary Fig. S8, at 400 MV m^{-1} (the maximum electric field allowed for the pristine terpolymer), despite the D value of the nanocomposite with 12 wt.% of BNNSs is below that of the pristine terpolymer, a larger integration area is clearly evident in the terpolymer nanocomposites as a consequence of the delayed *D*-saturation.

3.4. Thermal conductivity

An overlooked advantage of the dielectric polymer nanocomposites is considerably improved thermal conductivity when compared to that of pristine polymers. As dielectric loss is converted into waste heat, efficient dissipation of heat from dielectric materials to the external medium such as insulating oil is central to operation of capacitors. It is thus informative to examine the thermal conductivity of dielectric materials. Unfortunately, polymers are notoriously poor thermal conductors with thermal conductivities in the range of 0.1 - 0.5 W m^{-1} K^{-1} (ref. 42). As shown in Figure 5, with the introduction of BNNSs into the terpolymer matrix, the thermal conductivity is increased by 6 times from ~0.2 W m^{-1} K^{-1} of the terpolymer to over 1.4 W m^{-1} K^{-1} of the nanocomposite filled with 14 wt.% of BNNSs, which is close to those of barium titanate based ceramics (*i.e.* 1.1 - 6 W m^{-1} K^{-1}) (ref. 43).

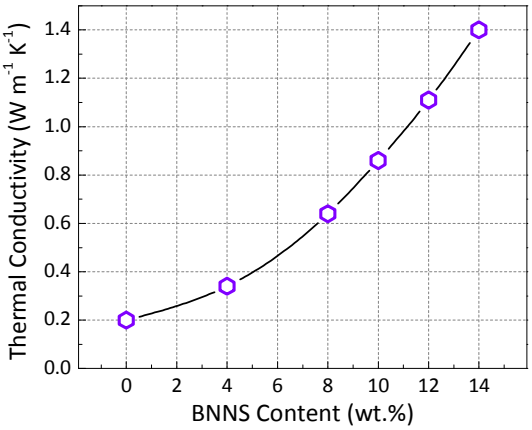

Fig.5 Thermal conductivity of P(VDF-TrFE-CFE)/BNNS nanocomposites with different filler contents.

4. Discussion

In an effort to understand the greatly improved E_b values, P(VDF-TrFE-CFE)/BNNS nanocomposites are systematically characterized in terms of mechanical properties, dissipation factor as well as electrical conduction. We first evaluated the Young's modulus of the materials because it determines the electromechanical failure caused by mutual coulombic force from the opposite electrodes under an applied field, *i.e.*, the higher the modulus is, the better the material can withstand the coulombic force.[44] As shown in Figure 6, the addition of BNNSs into the polymer matrix brings in significant enhancement in Young's modulus with the optimized composition at 12 wt.% of BNNSs, which agrees very well with the dependence of E_b on filler content shown in Figure 3b. We then calculated the theoretical E_b of the samples based on the electromechanical model according to: $E_b = 0.606(Y/(K\varepsilon_0))^{2/3}$, where Y is the Young's modulus and ε_o is the permittivity of free space.[45, 46] The results summarized in Fig. 6 show that theoretically calculated E_b has a similar trend to experimental data with the highest value appearing at 12 wt.% loading of BNNSs. It is thus reasoned that BNNSs within the polymer matrix create a robust scaffold to hamper the onset of electromechanical failure. Analysis within the framework of electromechanical model highlights the significance of the excellent mechanical strength of BNNSs for improving the E_b of ferroelectric polymers.

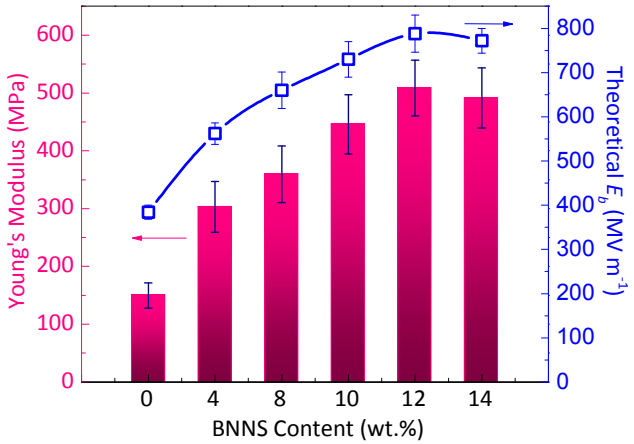

Fig.6 Young's modulus and theoretical data of breakdown strength calculated based on the electromechanical model of P(VDF-TrFE-CFE)/BNNS nanocomposites with different filler contents.

Note that the experimental data of Weibull E_b are much lower than the theoretically predicted values from the electromechanical model; this deviation is apparently due to limitations in the model. Many polymer materials do not exactly follow the elastic stress-strain relationship interpreted by the above equation, and would experience plastic deformation and mechanical failure at an electric field far below E_b (ref. 45). Furthermore, dielectric breakdown of materials is usually governed by multiple factors, although the electromechanical effect has been regarded as the main breakdown mechanism for PVDF based ferroelectric polymers. Dielectric materials studied by using the electromechanical model are in principle considered ideal insulators with the assumption of no electrical conduction under the applied fields. Electrical conduction, however, cannot be ignored in a real dielectric material, especially at high fields, and degrades dramatically the breakdown strength of materials.

Presented in Figures 7a and 7b are the weak-field dielectric loss and high-field electrical resistivity of the terpolymer nanocomposites, respectively. It is clear that the dielectric loss is sharply reduced from the pristine terpolymer to the nanocomposites, *e.g.* at 1 kHz, from 0.053 of the pristine terpolymer to 0.027 of the nanocomposite with 12 wt.% of BNNSs. Similarly, high-field DC conductivity measurements reveal that the terpolymer nanocomposites with high BNNS feeding ratios, *i.e.* >10 wt.%, show an order of magnitude improvement in electrical resistivity over that of the pristine terpolymer. These results indicate that the insulating network of BNNSs embedded in the polymer matrix function as efficient barrier against the leakage current and the space-charge conduction.

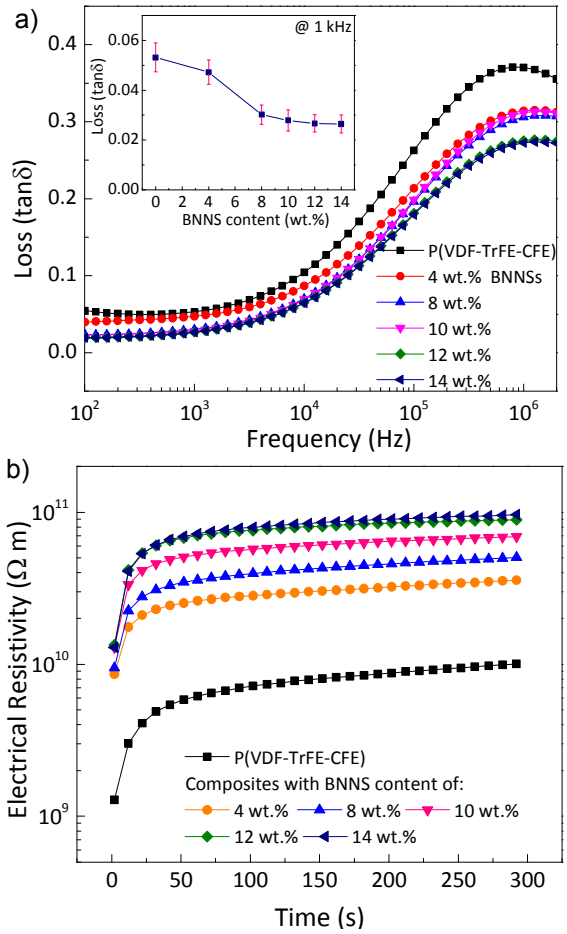

Fig.7 (**a**) Frequency dependence of dielectric loss of P(VDF-TrFE-CFE)/BNNS nanocomposites with different contents of BNNSs. Inset, dielectric loss of P(VDF-TrFE-CFE)/BNNS nanocomposites at 1 kHz as a function of filler content. (**b**) Electrical resistivity of P(VDF-TrFE-CFE)/BNNS nanocomposites with different contents of BNNSs under an electric field of 10 MV m^{-1}.

The reduction in remnant displacement by the presence of BNNSs is attributed to the suppressed conduction loss, as verified by the results of weak field loss and high field resistivity, and the decreased hysteresis loss that can be understood from the crystalline structures of the terpolymer. While the melt-stretching based processes convert partially the non-polar to polar phases of PVDF, the presence of BNNSs does not alter the crystalline phases of the polymer matrix. As shown in Fourier transform infrared (FTIR) spectra (Supplementary Fig. S9), the characteristic peaks corresponding to the T_3G, TG and T_m sequence conformations almost remain unaffected upon blending with BNNSs. In concert with the FTIR results, the reflection at 2θ = 18.1° arising from α or γ phase PVDF stays as the main peak in the X-ray diffraction (XRD) patterns of both the terpolymer and polymer nanocomposites (Supplementary Fig. S10). Note that the diffraction peak becomes broader as the filler content increases, which implies varied crystal size of the polymer in the nanocomposites. Quantitatively, the Scherrer equation was employed to calculate the apparent crystal size of the samples, since crystal size is an important factor determining the

reversibility of the dipoles within ferroelectric crystalline domains. Supplementary Information Table S1 shows a marked decrease in crystal size of the terpolymer nanocomposites compared to the pristine P(VDF-TrFE-CFE), *e.g.* from 49.4 nm of the pristine terpolymer to 29.0 nm of the nanocomposite with 12 wt.% of BNNSs. The crystals with reduced sizes shall facilitate the reverse of dipoles and thereby decrease the hysteresis loss.[47] Concurrently, the degree of crystallinity of polymer matrix is found to be slightly increased in the presence of BNNSs according to the enthalpy of melting extracted from the differential scanning calorimetry (DSC) curves (Supplementary Fig. S11 and Table S2). The inorganic nanosheets are thought to serve as nucleating agents to promote the population density of the nucleation centers for PVDF crystallization as implied by the elevated crystallization temperature (T_c) of the nanocomposites, *e.g.*, from 104 °C of the pristine terpolymers to 110 °C of the terpolymer nanocomposites with 12 wt% BNNSs. These results along with the decreased electrical conduction suggest that the introduction of BNNSs provides a feasible route for ferroelectric polymers to reduce energy loss and increase the charge-discharge efficiency for dielectric energy storage. In stark contrast, the improvements in E_b and U gained by mechanical stretching of dielectric films could be offset by the increase in high-field hysteresis loss and the reduction in charge-discharge efficiency arising from the evolution of the polar β phases at the expense of the nonpolar α phase.

We have also prepared BNNSs with different lateral sizes and thicknesses to assess the influence of filler dimension on dielectric properties of the polymer nanocomposites. The BNNSs include the smaller lateral size BNNSs (termed as sl-BNNSs, with an average lateral size of ~250 nm and thickness of ~2 nm, Supplementary Fig. S12) and two types of thicker BNNSs (referred to as 8t-BNNSs and 15t-BNNSs, for their average thicknesses of 8 and 15 nm, respectively, see Supplementary Fig. S13). It is found that sl-BNNS filled P(VDF-TrFE-CFE)s exhibit the same compositional dependent breakdown strength and the maximum breakdown field as the polymer nanocomposite loaded with regular size BNNSs with a lateral size of 400 nm and a thickness of 2 nm (Figure 8a). Accordingly, as shown in Figure 8b, P(VDF-TrFE-CFE)/sl-BNNS nanocomposites also display very high energy densities and charge-discharge efficiencies. On the other hand, the polymer nanocomposites with thicker BNNS fillers, i.e. 8t- and 15t-BNNSs, have lower Weibull breakdown strengths. At the same BNNS content, it appears that thinner fillers yield higher breakdown field of the nanocomposites (Figure 9). These results indicate that ultra-thin sheets are necessary, while the lateral dimension within a range from 250-400 nm may not be an important factor to determine the dielectric properties of the BNNS-doped ferroelectric polymers. Since lateral size of ultra-thin BNNSs is difficult to reach beyond this range via the liquid exfoliation method, it remains an open question if larger or smaller sheets could considerably affect the performance of the resulting nanocomposites.

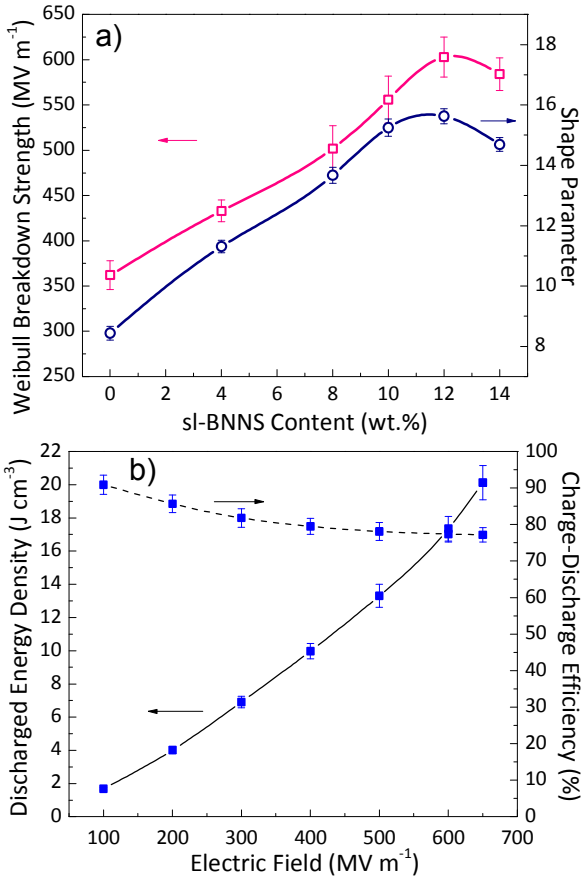

Fig. 8 (**a**) Weibull breakdown strength and shape parameter as functions of sl-BNNS fraction. (**b**) Discharged energy density and charge-discharge efficiency of P(VDF-TrFE-CFE)/sl-BNNS nanocomposites with 12 wt.% of sl-BNNSs at different electric fields.

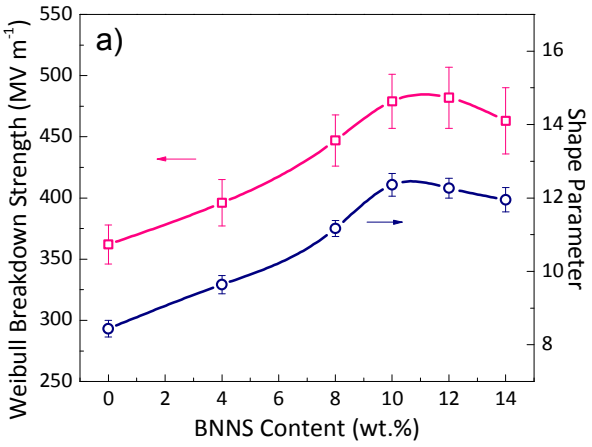

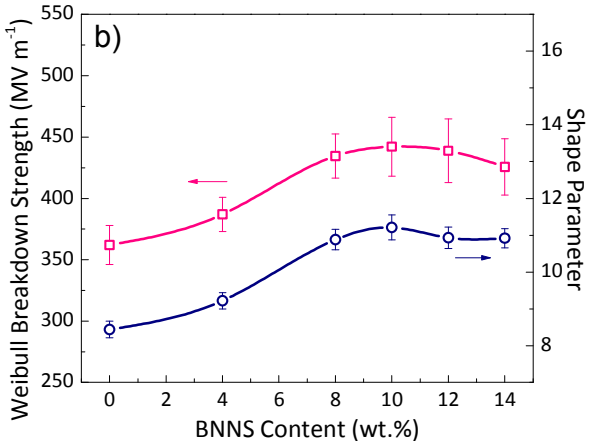

Fig. 9 Weibull breakdown strength and shape parameter as functions of BNNS content in (**a**) P(VDF-TrFE-CFE)/8t-BNNS and (**b**) P(VDF-TrFE-CFE)/15t-BNNS nanocomposites.

5. Conclusions

This work demonstrates the significantly enhanced dielectric breakdown strength, reduced energy loss, and improved charge-discharge efficiency of a ferroelectric terpolymer through incorporation of ultra-thin BNNSs, outperforming what can be achieved by melt-stretched and solution-cast pristine terpolymer. By capitalizing on the polar surface of the BNNSs with large specific surface area, the inorganic components are intimately and homogeneously dispersed in the polymer matrix without chemical surface modification. This renders a uniform and dense network of nanosheets against leakage current and space charge conduction that also acts as a robust scaffold to prevent electrochemical failure. Compared to the traditional melt-stretching or extrusion-blowing process used to produce high breakdown strength and high energy density dielectric polymer thin films, our approach is straightforward and versatile. Of particular significance is the considerably improved thermal conductivity of the terpolymer with the introduction of BNNSs, which is anticipated to benefit the breakdown stability and lifetime of polymer capacitors. The strategy presented herein could also have a profound impact on the applications of PVDF-based ferroelectric polymers in electrocaloric and pyroelectric energy conversions where concomitant enhancements in breakdown voltage and thermal conductivity are highly desired.

Acknowledgements

The authors gratefully acknowledge the support from the US office of Naval Research (N00014-11-1-0342) and the National Natural Science Foundation of China (No. 51072151, 51173139, 51373132).

Notes and references

[a] *Department of Materials Science and Engineering, The Pennsylvania State University, University Park, Pennsylvania, 16802, USA. E-mail: wang@matse.psu.edu*
[b] *School of Optical and Electronic Information, Huazhong University of Science and Technology, Wuhan, Hubei 430074, P. R. China*
[c] *State Key Laboratory of Advanced Technology for Materials Synthesis and Processing, and School of Materials Science and Engineering, Wuhan University of Technology, Wuhan 430070, People's Republic of China. E-mail: cxx@live.whut.edu.cn*
# These authors contribute equally to this work.
† Electronic Supplementary Information (ESI) available: structure characterizations, more dielectric property measurements and experimental details. See DOI: 10.1039/b000000x/

1. M. S. Whittingham, *MRS Bull.*, 2008, **33**, 411-419.
2. Y. Cao, P. C. Irwin, K. Younsi, *IEEE Trans. Dielect. Elect. Insul.*, 2004, **11**, 797-807.
3. S. Ducharme, *ACS Nano*, 2009, **3**, 2447-2450.
4. M. Rabuffi, G. Picci, *IEEE Trans. Plasma Sci.*, 2002, **30**, 1939-1942.
5. J. H. Pikul, H. G. Zhang, J. Cho, P. V. Braun, W. P. King, *Nature Commun.*, 2013, **4**, 1732.
6. M. F. El-Kady, V. Strong, S. Dubin, R. B. Kaner, *Science*, 2012, **335**, 1326-1330.
7. G. R. Love, *J. Am. Ceram. Soc.*, 1990, **73**, 323-328.
8. A. J. Lovinger, *Science*, 1983, **220**, 1115-1121.
9. H. S. Nalwa, *Ferroelectric Polymers*, Marcel Dekker, New York, 1995.
10. B. Chu, X. Zhou, K. Ren, B. Neese, M. Lin, Q. Wang, F. Bauer, Q. M. Zhang, *Science*, 2006, **313**, 334-336.
11. Z. Zhang, T. C. Chung, *Macromolecules*, 2007, **40**, 9391-9397.
12. Z. Zhang, Q. Meng, T. C. Chung, *Polymer*, 2009, **50**, 707-715.
13. X. Zhou, B. Chu, B. Neese, M. Lin, Q. M. Zhang, *IEEE Trans. Dielectr. Electr. Insul.*, 2007, **14**, 1133-1138.
14. X. Zhou, X. Zhao, Z. Suo, C. Zou, J. Runt, S. Liu, S. Zhang, Q. M. Zhang, *Appl. Phys. Lett.*, 2009, **94**, 162901.
15. P. Khanchaitit, K. Han, M. R. Gadinski, Q. Li, Q. Wang, *Nature Commun.*, 2013, **4**, 2845.
16. F. Xia, Z.-Y. Cheng, H. S. Xu, H. F. Li, Q. M. Zhang, G. J. Kavarnos, R. Y. Ting, G. Abdul-Sadek, K. D. Belfield, *Adv. Mater.*, 2002, **14**, 1574-1577.
17. H. Xu, Z.-Y. Cheng, D. Olson, T. Mai, Q. M. Zhang, G. Kavarnos, *Appl. Phys. Lett.*, 2001, **78**, 2360.
18. Y. Lu, J. Claude, B. Neese, Q. M. Zhang, Q. Wang, *J. Am. Chem. Soc.*, 2006, **128**, 8120-8121.
19. B. Chu, X. Zhou, B. Neese, Q. M. Zhang, F. Bauer, *IEEE Trans. Dielectr. Electr. Insul.*, 2006, **13**, 1162-1169.
20. N. Zebouchi, M. Bendaoud, R. Essolbi, D. Malec, B. Ai, H. Giam, *J. Appl. Phys.*, 1996, **79**, 2497-2501.
21. Q. Wang, L. Zhu, *J. Polym. Sci. Part B: Polym. Phys.*, 2011, 49, 1421-1429.
22. Z. M. Dang, J. Yuan, S. H. Yao, R. J. Liao, *Adv. Mater.*, 2013, 25, 6334-6365.
23. M. Roy, J. K. Nelson, R. K. MacCrone, L. S. Schadler, C. W. Reed, R. Keefe, W. Zenger, *IEEE Trans. Dielectr. Electr. Insul.*, 2005, **12**, 629-643.
24. M. Takala, H. Ranta, P. Nevalainen, P. Pakonen, J. Pelto, M. Karttunen, S. Virtanen, V. Koivu, M. Pettersson, B. Sonerud, K. Kannus, *IEEE Trans. Dielectr. Electr. Insul.*, 2010, **17**, 1259-1267.
25. V. Tomer, G. Polizos, C. A . Randall, E. Manias, *J. Appl. Phys.*, 2011, **109**, 074113.
26. S. P. Fillery, H. Koerner, L. Drummy, E. Dunkerley, M. F. Durstock, D. F. Schmidt, R. A. Vaia, *ACS Appl. Mater. Interfaces*, 2012, **4**, 1388-1396.

27. V. Tomer, E. Manias, C. A. Randall, *J. Appl. Phys.*, 2011, **110**, 044107.
28. C. Zhi, Y. Bando, C. C. Tang, H. Kuwahara, D. Golberg, *Adv. Mater.*, 2009, **21**, 2889-2893.
29. J. N. Coleman, M. Lotya, A. O'Neill, S. D. Bergin, P. J. King, U. Khan, K. Young, A. Gaucher, S. De, R. J. Smith, I. V. Shvets, S. K. Arora,G. Stanton, H.-Y. Kim, K. Lee, G. T. Kim, G. S. Duesberg, T. Hallam,J. J. Boland, J. J. Wang, J. F. Donegan, J. C. Grunlan, G. Moriarty, A. Shmeliov, R. J. Nicholls, J. M. Perkins, E. M. Grieveson, K. Theuwissen, D. W. McComb, P. D. Nellist, V. Nicolosi, *Science*, 2011, **331**, 568-571.
30. Q. Li, K. Han, M. R. Gadinski, G. Z. Zhang, Q. Wang, *Adv. Mater.* 2014, **26**, 6244.
31 F. Bauer, E. Fousson, Q. M. Zhang, L. M. Lee., *IEEE Trans. Dielectr. Electr. Insul.*, 2004, **11**, 293-298.
32. Y. Lu, J. Claude, Q. M. Zhang , Q. Wang , *Macromolecules* 2006, **39**, 6962.
33. H. Sahin, S. Cahangirov, M. Topsakal, E. Bekaroglu, E. Akturk, R. T. Senger, S. Ciraci. *Phys. Rev. B: Condens. Matter Mater. Phys.*, 2009, **80**, 155453.
34. D. Golberg, Y. Bando, Y. Huang, T. Terao, M. Mitome, C. Tang, C. Zhi, *ACS Nano*, 2010, **4**, 2979-2993.
35. C. R. Dean, A. F. Young, I. Meric, C. Lee, L. Wang, S. Sorgenfrei, K. Watanabe, T. Taniguchi, P. Kim, K. L. Shepard, J. Hone, *Nat. Nanotech.*, 2010, **5**, 722-726.
36. A. F. Young, C. R. Dean, I. Meric, S. Sorgenfrei, H. Ren, K. Watanabe, T. Taniguchi, J. Hone, K. L. Shepard, P. Kim, *Phys. Rev. B*, 2012, **85**, 235458.
37. J. E. Padilha, R. B. Pontes, A. Fazzio, *J. Phys.: Condens. Matter*, 2012, **24**, 075301.
38. K. R. Paton, *et al. Nat. Mater.* 2014, **13**, 624-630.
39. J. Y. Li, L. Zhang, S. Ducharme, *Appl. Phys. Lett.*, 2007, **90**, 132901.
40. F. X. Guan, L. Y. Yang, J. Wang, B. Guan, K. Han, Q. Wang, L. Zhu, *Adv. Funct. Mater.*, 2011, **21**, 3176-3188.
41. X. Zhou, *Doctoral thesis*, The Pennsylvania State University, December, 2009.
42. C. L. Choy, *Polymers*, 1977, **18**, 984-1004.
43. Y. S. Touloukian, R. W. Powell, C. Y. Ho, P. G. Klemens, *Thermophysical Properties of Matter*, IFI/Plenum Press, New York, 1970.
44. J. Claude, Y. Lu, Q. Wang, *Appl. Phys. Lett.*, 2007, **91**, 212904 .
45. K. H. Stark, C. G. Garton, *Nature*, 1955, **176**, 1225-1226.
46. M. Ieda, *IEEE Trans. Dielectr. Electr. Insul.*, 1980, **15**, 206-224.
47. J. Li, S. I. Seok, B. J. Chu, F. Dogan, Q. M. Zhang, Q. Wang, *Adv. Mater.*, 2009, **21**, 217-221.

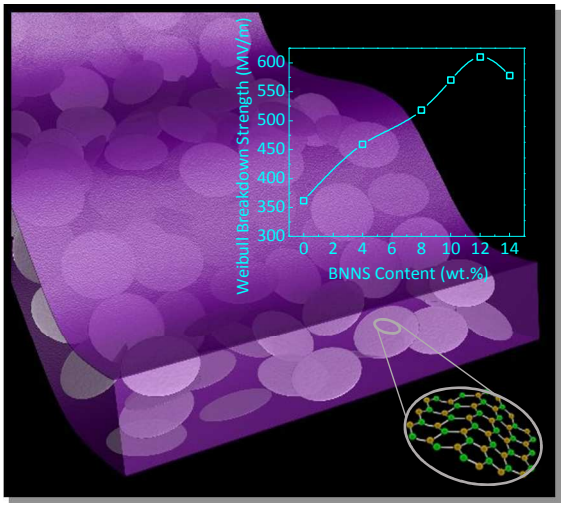

Ferroelectric polymer nanocomposites with boron nitride nanosheets exhibit greatly improved energy densities and higher charge-discharge efficiencies